Sensors and Materials, Vol. 38, No. 6 (2026) 3007–3014
MYU Tokyo

S & M 4483

Ni–Fe Layered Double Hydroxide @ Nickel Foam Electrode with Electrochemical Impedance Spectroscopy-based Performance Monitoring for Efficient Water Splitting

Hao-Ming Deng, Guan-Yu Chen, and Shih-Chen Shi*

Department of Mechanical Engineering, National Cheng Kung University (NCKU),
No. 1, University Road, Tainan 70101, Taiwan

(Received October 6, 2025; accepted February 16, 2026)

Keywords: Ni–Fe layered double hydroxide (LDH), electrochemical impedance spectroscopy (EIS), water splitting, charge-transfer resistance

Hydrogen energy is recognized as a clean and sustainable alternative to fossil fuels, but its large-scale production remains limited by the cost and stability of electrocatalysts. In this study, Ni–Fe layered double hydroxide–modified nickel foam (Ni–Fe LDH@NF) was synthesized by the hydrothermal method and evaluated as a bifunctional electrode for water splitting. Electrochemical impedance spectroscopy (EIS) was employed to investigate charge-transfer behavior and interfacial resistance during operation. Nyquist plots showed that the electronic coupling between Ni and Fe significantly enhanced electron transport. At the same time, prolonged reaction time increased the charge-transfer resistance (R_{ct}) because of surface oxidation and by-product accumulation. A linear relationship between R_{ct} and reaction time was established, enabling the use of EIS data for the lifetime prediction of the electrode. Scanning electron microscopy revealed the structural degradation of the LDH layer after extended electrolysis, which is consistent with the impedance results. These findings demonstrate that Ni–Fe LDH@NF exhibits high catalytic efficiency and moderate durability for alkaline water splitting. The proposed EIS-based "sensing–diagnosis prediction" approach provides a quantitative method for evaluating electrode stability. This work suggests that Ni–Fe LDH is a promising non-noble metal catalyst and diagnostic sensor for future hydrogen energy applications.

1. Introduction

The global energy demand continues to rise as population growth and industrialization accelerate. Fossil fuels remain the dominant energy source, but their overuse causes environmental pollution, climate change, and the gradual depletion of finite resources. Hydrogen energy, with high energy density and water as its single combustion product, is widely recognized as the "ultimate clean energy". However, most hydrogen is still produced via fossil-fuel reforming, which emits large amounts of CO_2 and undermines sustainability goals. In

*Corresponding author: e-mail: scshi@mail.ncku.edu.tw
https://doi.org/10.18494/SAM5964

ISSN 0914-4935
https://myukk.org/

contrast, “green hydrogen”, produced via water electrolysis powered by renewables, achieves zero carbon emissions at the source and mitigates fluctuations in fossil fuel pricing. According to Deloitte’s Global Green Hydrogen Outlook Report (2023),[1] the global hydrogen market is projected to reach USD 1.4 trillion by 2050, with the Asia–Pacific region accounting for ~USD 645 billion, highlighting vast growth potential.

Recent advances in sustainable materials and nanotechnology suggest that structure, composition, and interface engineering can critically affect performance in energy systems. Studies on rice-straw-derived chitosan plasticizers and cellulose/aluminum nanocomposites illustrate how biomass-based components can enhance material robustness and interface compatibility.[2,3] Works on InN nanostructures with temperature-quenched photoluminescence and TEMPO-oxidized cellulose films via different processing routes emphasize that nanoscale control and processing strategies significantly affect functional behaviors—an insight transferable to electrocatalyst design.[4,5]

Numerous studies have explored catalysts for hydrogen evolution reaction (HER) and oxygen evolution reaction (OER) in electrocatalysis. Noble metals such as RuO_2, IrO_2, and Pt show excellent activity and stability,[6,7] but their high cost and scarcity hinder large-scale deployment. Thus, the research focus has shifted toward non-noble metal systems, with Ni–Fe layered double hydroxides (LDHs) emerging as a leading candidate due to tunable composition, high surface area, and layered interfacial architectures.[8] A comprehensive review has recently summarized strategies including morphology control, doping, defect engineering, and heterostructure design in NiFe LDHs.[6] For instance, the Ce-doped NiFe LDH grown *in situ* on Ni foam reduced overpotential and stabilized catalytic performance,[6] whereas the Ti_3C_2 mediation of NiFe-LDH enhanced OER kinetics.[9] Nb doping (Nb/NiFe-LDH) was reported to induce electron-deficient Ni species and accelerate phase reconstruction during OER.[10] Heterostructured NiFe@NiB improved durability and reduced Fe leaching.[11] The scalable synthesis of NiFe-LDH under room temperature and atmospheric conditions further enabled practical deployment in full-cell electrolyzers.[12] Recent reviews addressed iron leaching, phase transitions, and structural degradation to manage stability issues.[13] Functional coupling with Ru single atoms anchored on NiFe LDH (via oxygen coordination) further enhanced water oxidation performance.[14] New approaches, such as Mo doping to activate lattice oxygen,[15] S modification of NiFe LDH,[16] and multi-heterojunction designs such as Ru/Ni_3S_2/NiFe LDH for bifunctional catalysis,[17] have also been developed. Continuous hydrothermal flow synthesis (CHFS) enables the stable production of 2D NiFe hydroxide materials at scale.[18] On model surfaces, Ni-modified Fe_3O_4(001) has been used to probe the synergy of Fe and Ni in OER and EIS behavior.[19]

In this study, we aim to analyze Ni–Fe LDH-modified Ni foam (Ni–Fe LDH@NF) electrodes by electrochemical impedance spectroscopy (EIS) to probe interfacial charge transfer, reaction kinetics, and long-term stability. The results reveal that Ni–Fe LDH@NF exhibits excellent charge-transfer capability, low impedance, robust electrocatalytic activity, and structural durability, supporting its promise as a practical, non-noble metal catalyst for green hydrogen generation.

2. Materials and Methods

2.1 Synthesis of Ni–Fe LDH

Nickel nitrate (1.495 g), iron nitrate (0.6925 g), ammonium fluoride (0.635 g), and urea (2.059 g) were dissolved in 120 g of deionized (DI) water under stirring. A piece of nickel foam (NF) was immersed in the Ni–Fe solution and transferred to a Teflon-lined autoclave sealed with Teflon tape. The hydrothermal reaction proceeded at 120 °C for 12 h. After cooling to 60 °C, the product was rinsed repeatedly with DI water until neutral pH and dried at 60 °C for 48 h, yielding Ni–Fe layered double hydroxide-modified nickel foam (Ni–Fe LDH@NF).

2.2 Hydrogen evolution test

Hydrogen generation was evaluated in an electrolytic cell using two inverted graduated cylinders. Ni–Fe LDH@NF electrodes were connected to clips and positioned in separate cylinders. A constant current of 8 mA was applied, and variations in liquid level were monitored to assess hydrogen evolution performance.

2.3 EIS

EIS was conducted to examine charge-transfer resistance and interfacial properties. Ni–Fe LDH@NF (0.5 × 2 cm^2) served as the working electrode, the saturated calomel electrode (SCE) as the reference electrode, and a platinum plate as the counter electrode. Measurements were performed in 1 M KOH solution from 0.1 Hz to 100 kHz with an AC amplitude of 10 mV. Impedance data were analyzed to evaluate electron-transfer efficiency.

To quantitatively analyze the impedance behavior, the EIS spectra were fitted using a modified Randles equivalent circuit model.[20] The circuit consisted of the solution resistance (R_s), charge-transfer resistance (R_{ct}), and a constant phase element (CPE) to account for the non-ideal capacitive characteristics of the electrode/electrolyte interface.

2.4 Characterization

FE-SEM (JEOL JSM-7600F) observed the surface morphology and composition with EDS mapping, confirming uniform nanosheet growth on Ni foam. XRD (Bruker D8 Advance, Cu Kα = 1.5406 Å) and FTIR (Thermo Nicolet iS10, 4000–400 cm^{-1}) identified crystal structure and bonding. XPS (PHI 5000 VersaProbe III) characterized surface states, whereas BET analysis (Micromeritics TriStar II 3020) provided surface area and pore data. Electrochemical measurements including cyclic voltammetry (CV), linear sweep voltammetry (LSV), and EIS were performed using a CHI 760E workstation. The resulting Tafel slope and Nyquist plots revealed low charge-transfer resistance and efficient electron transport, confirming the favorable electrochemical kinetics of Ni–Fe LDH@NF for hydrogen evolution.

3. Results and Discussion

3.1 Electrochemical impedance analysis

Figure 1 shows Ni–Fe LDH@NF and uncoated NF samples. The Ni–Fe LDH@NF film displayed a uniform golden surface, whereas the pristine NF film exhibited its native metallic luster. This contrast confirms that the LDH coating adhered evenly and altered the substrate's optical appearance.

EIS was used to evaluate the electrodes' charge-transfer behavior and verify their catalytic activity. Nyquist plots for different reaction times are shown in Fig. 2(a), and the corresponding equivalent circuit is presented in Fig. 2(b). The semicircular arcs indicate that the interfacial reaction was mainly controlled by the charge-transfer process at the electrode electrolyte interface.

The semicircle diameters were small at 0 and 1 h, and the corresponding R_{ct} values were below 250 Ω. These results indicate that abundant active sites on the Ni–Fe LDH surface enabled efficient electron transport and rapid oxidation reactions. The observation agrees with previous findings that electronic coupling between Ni and Fe species enhances interfacial charge transfer and reduces reaction barriers. As the reaction time increased to 3 and 4 h, the semicircular arcs expanded and R_{ct} rose to approximately 300–400 Ω. The gradual increase suggests that surface reactions became limited as oxygenated intermediates or by-products such as NiOOH accumulated and covered active regions. This surface reconstruction reduced the number of

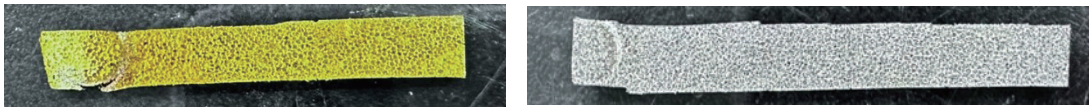

(a) (b)

Fig. 1. (Color online) (a) Ni–Fe LDH@NF film and (b) NF film.

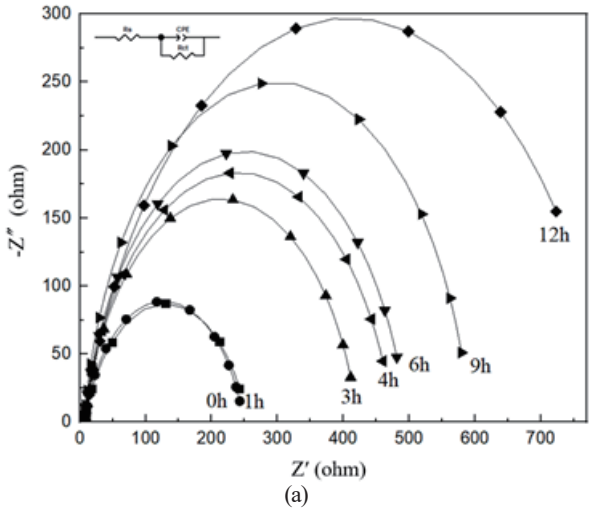

(a)

material	Z′(ohm)
NiFe LDH-0h	242.49
NiFe LDH-1h	242.79
NiFe LDH-3h	411.36
NiFe LDH-4h	460.12
NiFe LDH-6h	481.44
NiFe LDH-9h	579.49
NiFe LDH-12h	723.23

(b)

Fig. 2. (a) Nyquist plots of Ni–Fe LDH@NF at different reaction times and (b) equivalent circuit model and impedance variation with time.

accessible catalytic sites and led to lower electrochemical activity over time. When the duration extended to 6, 9, and 12 h, the Nyquist semicircles enlarged significantly, with R_{ct} reaching 500–700 Ω. The increase demonstrates that interfacial resistance dominated at longer operation times, suppressing charge-transport efficiency. These results reveal that prolonged electrolysis caused the structural degradation of the Ni–Fe LDH layer, posing a stability challenge for extended hydrogen production.

3.2 EIS-based sensor analysis and surface morphology evolution

Figure 3(a) shows EIS data processed for sensor-based analysis. The linear correlation between R_{ct} and reaction time ($y = 38.54x + 258.23$) confirms that impedance variations can quantify performance decay. The relation demonstrates that EIS can be a predictive diagnostic tool for monitoring electrode durability and degradation behavior. SEM observations revealed the microstructural evolution of Ni–Fe LDH@NF during operation. Initially, Ni–Fe LDH nanosheets uniformly covered the Ni foam skeleton, forming a porous and interconnected architecture that maximized the active surface area. After 12 h, surface deposits and localized agglomerations appeared, while cracks formed in the Ni foam framework, indicating progressive structural fatigue.

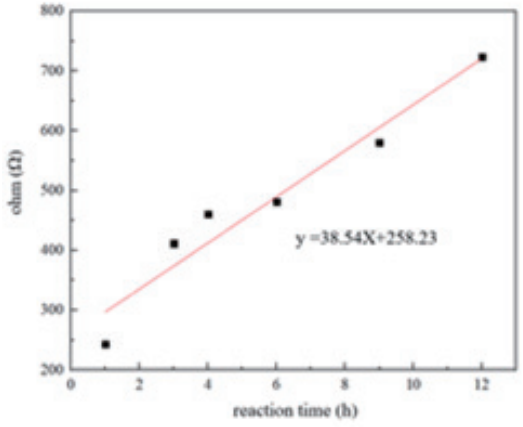

(a)

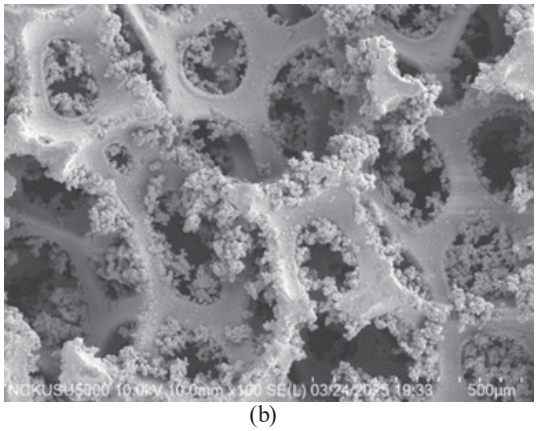

(b)

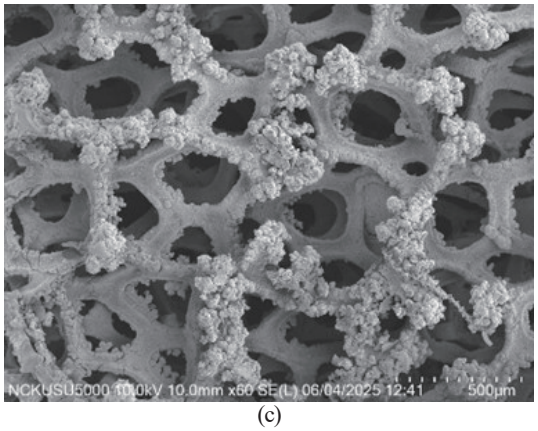

(c)

Fig. 3. (a) EIS calibration curve, (b) SEM image of Ni–Fe LDH@NF after 0 h, and (c) SEM image of Ni–Fe LDH@NF after 12 h.

These morphological changes explain the increased R_{ct} and reduced catalytic efficiency observed in Fig. 2. The accumulation of oxide intermediates and physical damage hindered electron transport and bubble release. Consequently, the effective reaction area decreased, leading to slower charge transfer and lower hydrogen evolution efficiency.

In addition to the 12 h electrochemical operation, short-term immersion and thermal perturbation observations indicated that the Ni–Fe LDH layer remained well adhered to the Ni foam substrate without notable peeling or delamination. Although extended long-term cycling was not performed in this study, these preliminary results suggest that the interface retains adequate mechanical integrity during early-stage operation. More comprehensive thermal and chemical aging tests will be conducted in future work to fully validate the long-term robustness of the Ni–Fe LDH@NF interface.

The correlation between impedance growth and surface deterioration highlights the role of EIS as an *in situ* monitoring technique. Tracking R_{ct} in real time can quantitatively assess and predict the electrode's activity through the established linear model. Such sensing, diagnosis, and prediction integration offers valuable insight for the operational maintenance of hydrogen electrolysis systems. The performance decay observed here has been consistent with previous studies of Ni–Fe LDH electrodes under alkaline conditions. Long-term exposure to OH^- ions and oxidation cycles has been reported to cause the partial dissolution and restructuring of LDH layers. Therefore, enhancing corrosion resistance and surface integrity remains critical for industrial-scale hydrogen generation.

The comparative analysis of earlier reports has shown that element doping and hybrid structures can improve long-term stability. Strategies such as incorporating Ce or Nb dopants have reduced R_{ct} and slowed degradation by modulating electronic states. These improvements suggest that compositional control can counteract the time-dependent impedance growth observed in this study. In this work, Ni–Fe LDH@NF maintained active catalytic sites during the early stages of operation, confirming its high initial efficiency. However, prolonged operation led to the formation of passivation layers that limited conductivity and catalytic turnover. The results demonstrate the trade-off between initial activity and long-term durability for Ni–Fe LDH catalysts. The EIS-based monitoring model provides a practical approach for predicting electrode lifespan in real electrolysis systems. The strong linearity between reaction time and impedance enables the early detection of performance loss before severe degradation occurs. This predictive capability offers practical value for optimizing replacement schedules and reducing maintenance costs.

Ni–Fe LDH@NF showed excellent initial conductivity, rapid charge transfer, and structural uniformity. Nevertheless, the gradual increase in R_{ct} revealed its susceptibility to surface reconstruction and mechanical fatigue under prolonged electrolysis. Addressing these issues through structural stabilization and compositional tuning will be vital for advancing Ni–Fe LDH electrodes toward practical hydrogen energy applications.

4. Conclusions

In this study, we demonstrated that Ni–Fe LDH exhibits high catalytic activity and stable operation during water-splitting reactions. Electrochemical impedance spectroscopy (EIS) results revealed that the strong electronic coupling between Ni and Fe effectively facilitates charge transfer and reduces interfacial resistance. However, prolonged electrolysis leads to the accumulation of oxygenated by-products, which increases impedance and limits long-term catalytic efficiency. These findings confirm that the linear regression model derived from R_{ct} variations is a reliable tool for evaluating electrode lifetime, and the proposed "sensing–diagnosis–prediction" framework establishes an integrated approach for the real-time monitoring of catalytic performance. Although the Ni–Fe LDH electrode shows moderate durability during the early stages of operation, the progressive rise in impedance indicates that its long-term structural and catalytic stability requires further enhancement. Overall, Ni–Fe LDH shows considerable potential as a cost-effective and durable non-noble-metal catalyst with dual electrocatalytic and sensing functionalities.

Impedance measurements were performed under fixed conditions (1 M KOH, 25 °C, and a static electrolyte), and the effects of electrolyte pH, temperature, and flow rate on impedance responses or sensing reproducibility were not systematically investigated. We acknowledge that these environmental and operational factors may affect EIS outcomes. Therefore, future work will focus on evaluating how electrolyte acidity/alkalinity, operating temperature, and static versus dynamic flow environments regulate measurement stability and accuracy.

Furthermore, upcoming efforts will also aim to enhance the structural stability, durability, and scalability of Ni–Fe LDH electrodes for industrial hydrogen production. Approaches such as incorporating carbon-based supports, applying heterostructure engineering, and introducing surface modification strategies will be adopted to improve mechanical integrity and corrosion resistance. With the continued optimization of both operating conditions and material design, Ni–Fe LDH systems are expected to emerge as strong candidates for next-generation sustainable energy conversion technologies.

Acknowledgments

This work was supported by the National Science and Technology Council (NSTC), Taiwan, under Grant Nos. 113-2221-E-006-087-MY2, 113-2221-E-006-112-MY2, and 114-2221-E-006-090. The authors also acknowledge the Core Facility Center of National Cheng Kung University (NCKU), Taiwan, for providing access to EM000600, funded by NSTC project 114-2740-M-006-001. Additional support from the Higher Education Sprout Project, Ministry of Education, Taiwan, through the Headquarters of University Advancement at NCKU, is gratefully acknowledged.

References

1 D. Franzmann, H. Heinrichs, F. Lippkau, T. Addanki, C. Winkler, P. Buchenberg, T. Hamacher, M. Blesl, J. Linßen, and D. Stolten: Int. J. Hydrogen Energy **48** (2023) 33062.
2 S.-C. Shi, T.-H. Chen, and P. K. Mandal: Polymers **12** (2020) 1246.
3 S.-C. Shi, F.-I. Lu, C.-Y. Wang, Y.-T. Chen, K.-W. Tee, R.-C. Lin, H.-L. Tsai, and D. Rahmadiawan: Int. J. Biol. Macromol. **264** (2024) 130547.
4 D. Rahmadiawan, S.-C. Shi, H. Abral, M. K. Ilham, E. Sugiarti, A. N. Muslimin, R. Ilyas, R. Lapisa, and N. S. D. Putra: J. Natural Fibers **21** (2024) 2301386.
5 S.-C. Shi, C.-F. Chen, G.-M. Hsu, J.-S. Hwang, S. Chattopadhyay, Z.-H. Lan, K.-H. Chen, and L.-C. Chen: Appl. Phys. Lett. **87** (2005) 203103.
6 P. M. Bodhankar, P. B. Sarawade, G. Singh, A. Vinu, and D. S. Dhawale: J. Mater. Chem. A **9** (2021) 3180.
7 D. P. Sahoo, K. K. Das, S. Mansingh, S. Sultana, and K. Parida: Coord. Chem. Rev. **469** (2022) 214666. https://doi.org/10.1016/j.ccr.2022.214666
8 H. Sun, W. Zhang, J.-G. Li, Z. Li, X. Ao, K.-H. Xue, K. K. Ostrikov, J. Tang, and C. Wang: Appl. Catal. B **284** (2021) 119740.
9 Y. Sun, Z. Wang, Q. Zhou, X. Li, D. Zhao, B. Ding, and S. Wang: Heliyon **10** (2024).
10 B. Ding, Z. Jiang, X. Guo, S. Wen, K. Wang, S. Li, Y. Yang, Q. Sha, B. Li, and L. Luo: Nanoscale **17** (2025) 7825.
11 J. Lim, S. Jo, H. Oh, P. Choi, J. Oh, K. Seo, H.-Y. Park, and K. Eom: J. Mater. Chem. A **13** (2025) 33479.
12 A. Seijas-Da Silva, A. Hartert, V. Oestreicher, J. Romero, C. Jaramillo-Hernández, L. J. Muris, G. Thorez, B. J. Vieira, G. Ducourthial, and A. Fiocco: Nat. Commun. **16** (2025) 6138.
13 Y. Han, J. Wang, Y. Liu, T. Li, T. Wang, X. Li, X. Ye, G. Li, J. Li, and W. Hu: Carbon Neutralization **3** (2024) 172.
14 Y. Yang, Q.-N. Yang, Y.-B. Yang, P.-F. Guo, W.-X. Feng, Y. Jia, K. Wang, W.-T. Wang, Z.-H. He, and Z.-T. Liu: ACS Catalysis **13** (2023) 2771.
15 L. Wei, M. Du, R. Zhao, F. Lv, L. Li, L. Zhang, D. Zhou, and J. Su: J. Mater. Chem. A **10** (2022) 23790.
16 J. Long, J. Zhang, L. Li, Y. Wen, X. Xu, and F. Wang: Int. J. Hydrogen Energy **90** (2024) 1424.
17 Y. Tian, J. Li, F. Li, R. Wang, J. Liu, and J. Ma: Ind. Eng. Chem. Res. **64** (2025) 15165.
18 M. Rosa, D. Marani, G. Perin, S. B. Simonsen, P. Zielke, A. Glisenti, R. Kiebach, A. Lesch, and V. Esposito: React. Chem. Eng. **4** (2019) 2060.
19 F. Mirabella, M. Müllner, T. Touzalin, M. Riva, Z. Jakub, F. Kraushofer, M. Schmid, M. T. Koper, G. S. Parkinson, and U. Diebold: Electrochim. Acta **389** (2021) 138638.
20 S. Das, A. Banerjee, U. Nandi, and A. Ghosh: J. Appl. Phys. **138** (2025) 125002.